Metallic Coulomb blockade thermometry down to 10 mK and below

L. Casparis,[1] M. Meschke,[2] D. Maradan,[1] A. C. Clark,[1,a)] C. P. Scheller,[1]
K. K. Schwarzwälder,[1] J. P. Pekola,[2] and D. M. Zumbühl[1,b)]
[1]*Department of Physics, University of Basel, CH-4056 Basel, Switzerland*
[2]*Low Temperature Laboratory (OVLL), Aalto University, 00076 Aalto, Finland*

(Received 8 June 2012; accepted 25 July 2012; published online 15 August 2012)

We present an improved nuclear refrigerator reaching 0.3 mK, aimed at microkelvin nanoelectronic experiments, and use it to investigate metallic Coulomb blockade thermometers (CBTs) with various resistances R. The high-R devices cool to slightly lower T, consistent with better isolation from the noise environment, and exhibit electron-phonon cooling $\propto T^5$ and a residual heat-leak of 40 aW. In contrast, the low-R CBTs display cooling with a clearly weaker T-dependence, deviating from the electron-phonon mechanism. The CBTs agree excellently with the refrigerator temperature above 20 mK and reach a minimum-T of 7.5 ± 0.2 mK. © *2012 American Institute of Physics*. [http://dx.doi.org/10.1063/1.4744944]

Advancing to ever lower temperatures can open the door for the discovery of new physics: for example, submillikelvin temperatures in quantum transport experiments could lead to novel nuclear-spin physics[1,2] in nanoscale semiconductor devices[3] or could facilitate the study of non-Abelian anyons, Majorana fermions and topological quantum computation in fractional quantum Hall samples.[4,5] However, cooling of nanoscale devices below $T \sim 1$ mK is a formidable challenge due to poor thermal contact as well as microwave and other heating, often resulting in device and/or electron temperatures raised well above the refrigerator temperature. Therefore, significant progress beyond the status quo in both cooling techniques and thermometry is necessary.

One approach to overcome these difficulties uses Ag sinters[6–8] to thermalize the sample wires,[9] pioneered by the Florida group.[10,11] Another approach—pursued by our Basel group[12]—is to use nuclear cooling[6–8] on the sample wires, with the potential to advance well into the microkelvin range. Thermometry in this regime[6–8] typically faces similar challenges as cooling nanostructures and is ideally integrated on-sample. Among numerous sensors,[13] Coulomb blockade thermometers[14] (CBTs) are simple to use and self-calibrating yet offer high accuracy, demonstrated down to ∼20 mK.[15] Here, we present an improved nuclear refrigerator (NR) for cooling nanoelectronic samples and use it to investigate CBTs and their mechanisms of cooling.

We employ a novel scheme for cooling electronic nanostructures into the microkelvin regime by thermalizing each sample wire directly to its own, separate nuclear refrigerator.[12] In this scheme, the sample cools efficiently through the highly conducting wires via electronic heat conduction, bypassing the phonon degree of freedom since it becomes inefficient for cooling at low T. A prototype of this refrigerator presented in Ref. 12 has been significantly improved in a second generation system, briefly outlined below and in Fig. 1. A network of 21 parallel NRs is mounted on a rigid tripod intended to minimize vibrational heating. Two separate 9 T magnets allow independent control of the NR and sample magnetic field.

Several stages of thermalization and filtering are provided on each sample wire (see Fig. 1). After π-filters and thermocoax,[16] each lead passes through a Ag-epoxy microwave filter,[17] followed by a RC filter. Each wire then feeds into a Ag-sinter in the mixing chamber, emerging as a massive high-conductivity Ag wire. After Al heat-switches with fused joints, each lead traverses a separate Cu-NR via spot-

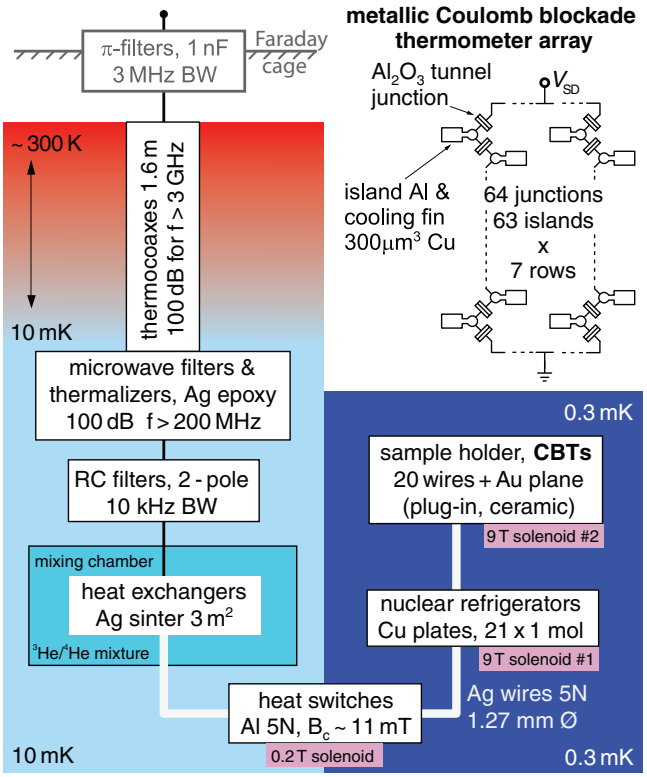

FIG. 1. Layout of novel nanosample microkelvin refrigerator and CBT array. Radiation shields (not drawn) are attached to the still and cold pate (∼50 mK). The RC filters are 820 Ω/22 nF and 1.2 kΩ/4.7 nF. The 21 NR plates are 0.25 × 3.2 × 9.0 cm^3 each, amounting to 64 g Cu per plate.

a)Also at Department of Geophysics, Stanford University, Stanford, USA.
b)Dominik.Zumbuhl@unibas.ch.

welded contacts, terminating in an easily-exchangeable chip carrier plugged into Au-plated pins which are spot welded to the Ag wires. Therefore, excellent thermal contact (<50 mΩ) is provided between the bonding pads and the parallel network of 21 Cu pieces—the microkelvin bath and heart of the nuclear refrigerator—while maintaining electrical isolation of all wires from each other and from ground, as required for nanoelectronic measurements.

The performance of the NRs is evaluated in a series of demagnetization runs. The temperature T_{Cu} of the Cu pieces is obtained using a standard technique:[7,8,12] after demagnetization, we apply power on heaters mounted on some of the NRs and evaluate the warm-up time-dependence $T_{Cu}(t)$ measured with Lanthanum Cerium Magnesium Nitrate (LCMN) thermometers above 2 mK. This allows us to determine both the temperature T_{Cu} of the Cu-NRs after demagnetization as well as a small field-offset. For each demagnetization run, the NRs are precooled to $T_i \sim 12$ mK in a $B_i = 9$ T magnetic field and then demagnetized to temperatures as low as $T_f \sim 0.3$ mK after the field has been slowly ramped down to $B_f \sim 0.135$ T, giving efficiencies $(T_i/T_f)/(B_i/B_f) \gtrsim 60\%$. Reruns showed excellent repeatability, allowing us to chart T_{Cu} for various B_f. To determine T_{Cu} during the CBT experiments, we use the LCMN thermometers above 2 mK, warm-up curves at the lowest B_f and in-between, the pre-charted T_{Cu} values.

The network with 21 NRs allows measurements of several CBTs (2-wire each). The CBT devices are Au-wire bonded and glued to the Au backplane of the chip carrier which is also cooled with a NR. Each CBT consists of 7 parallel rows of 64 Al/Al_2O_3 tunnel-junctions in series with an area of 2 μm^2 fabricated using e-beam lithography and shadow evaporation. The process used allows oxidation at elevated temperatures, giving junction resistances up to 1 MΩ μm^2. Each island extends into a large cooling fin made from Cu, since Cu gives excellent electron-phonon (EP) coupling. A small $B \sim 150$ mT is applied perpendicular to the sensor wafer to suppress the superconductivity of the Al. The differential conductance through a CBT sensor was measured with a standard lock-in technique adding a small ac excitation V_{ac} to a dc bias V_{SD}. Note that only 1/64 of the applied voltage drops across each junction and the sensor resistance R is 64/7 times the junction resistance R_j, assuming identical junctions.

We investigated CBTs with various R, see Fig. 2. Due to Coulomb blockade effects, the conductance around zero bias $V_{SD} = 0$ is suppressed below the large-bias conductance g_T. Both width and depth $\delta g = 1 - g(V_{SD} = 0)/g_T$ of the conductance dip are related to the CBT electron temperature T_{CBT}. To extract T_{CBT}, we perform fits (dashed curves) using a numerical model from Ref. 18. We find excellent agreement between model and data (see Fig. 2). Independently, T_{CBT} can be obtained[18] from the conductance dip $\delta g = u/6 - u^2/60 + u^3/630$ with $u = E_C/(k_B T_{CBT})$ and charging energy E_C. We first extract E_C at high-T assuming $T_{Cu} = T_{CBT}$ and then use this E_C to extract T_{CBT} from δg everywhere. While both methods produce very similar T_{CBT} (deviating slightly only at the lowest T), the δg approach makes no *a priori* assumptions about the cooling mechanism, allowing us an unbiased investigation, though now requiring high-T calibration against another thermometer. All T_{CBT} values given here are from the δg method.

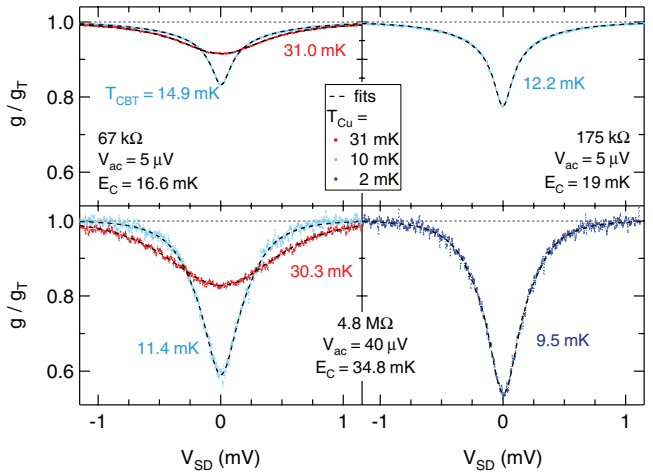

FIG. 2. CBT normalized differential conductance g/g_T versus source-drain dc bias V_{SD} for various NR temperatures T_{Cu} as color-coded, with resulting T_{CBT} (δg method, see text) given adjacent to each trace. Data from a 67 kΩ, 175 kΩ, and 4.8 MΩ CBT is shown. Dashed curves are fits to a model (see text). Note lower noise in low-R sensors due to larger resulting currents.

The thermalization properties of T_{CBT} of the lowest and highest R CBTs are displayed in Fig. 3 for a wide range of T_{Cu} from 0.5 mK to 100 mK. As seen, excellent agreement is found between T_{CBT} and T_{Cu} at high temperatures, as expected. Further, T_{CBT} is seen to lie well above T_{Cu} at the lower temperatures (see Figs. 2 and 3), decoupling fully from T_{Cu} well below 10 mK. We note that V_{ac} was experimentally chosen to avoid self-heating. Also, the 4.8 MΩ sensor reaches lower temperatures than the other, lower impedance CBTs, consistent with better isolation from the environment, since the power dissipated is proportional to V_{env}^2/R_j, with environmental noise voltage V_{env}.

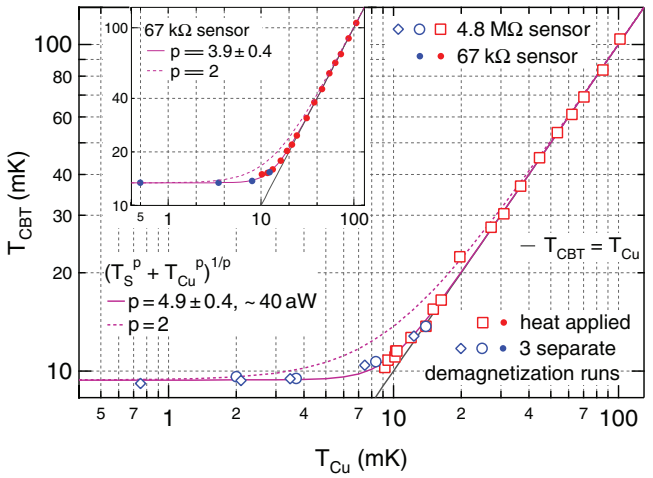

FIG. 3. CBT electron temperature T_{CBT} versus NR temperature T_{Cu} for 4.8 MΩ (open markers) and 67 kΩ sensors (filled markers, same axes on inset as main figure). Below 10 mK, the data are obtained in 3 demagnetization sweeps (blue markers) with $B = 9$ T, 5 T, 2 T, 1 T, and 0.4 T in a typical run, ramped at 1 T/h above 1 T and 0.5 T/h below. Error bars are about the size of the markers. Purple curves are T_{CBT} saturation curves (see text).

To model the CBT thermalization,[18] we write down the heat flow $\dot{Q}_i$ onto a single island i with electron temperature T_i:

$$\dot{Q}_i = \frac{V_j^2}{R_j} + \sum_{\pm} \frac{\pi^2 k_B^2}{6e^2 R_j}\left(T_{i\pm1}^2 - T_i^2\right) - \Sigma\Omega\left(T_i^5 - T_p^5\right) + \dot{Q}_0, \tag{1}$$

where $\dot{Q}_0$ is a parasitic heat leak and V_j is the voltage drop across the junction, appearing here in the Joule heating term. Σ is the Cu EP coupling constant, $\Omega = 300\,\mu\text{m}^3$ the island volume and T_p the phonon bath temperature assumed to be equal to T_{Cu}. This is well justified by the high thermal conductance between the NRs and bonding pads. Note that at $T \ll 1\,\text{K}$, the sample-to-Au-backplane interface resistance (Kapitza) is small compared to the EP coupling resistance.[18] Within this model, two cooling mechanisms are included: Wiedemann-Franz (WF, T^2 term) and EP cooling. Note the strong T^5 dependence of the EP term, ultimately rendering WF cooling dominant at sufficiently low T. Assuming one mechanism and simplifying to only one island gives a saturation curve $T_{\text{CBT}} = (T_S^p + T_{\text{Cu}}^p)^{1/p}$, with a CBT saturation temperature T_S and an exponent p, corresponding to $p = 2$ for WF-electron cooling and $p = 5$ for EP cooling.

We study the mechanism of thermalization by fitting the saturation curve first to the 4.8 MΩ data. We find very good agreement, giving $p = 4.9 \pm 0.4$ (see Fig. 3), indicating that EP coupling presents the dominant cooling mechanism, limiting T_{CBT} to 9.2 mK even though $T_{\text{Cu}} = 0.75\,\text{mK}$. Using $\dot{Q}_0 = \Sigma\Omega T_{\text{CBT}}^5$, a small parasitic heat leak $\dot{Q}_0 = 40\,\text{aW}$ results for each island, with $\Sigma = 2 \times 10^9\,\text{Wm}^{-3}\text{K}^{-5}$ from Ref. 18. We speculate that $\dot{Q}_0$ could be caused by electrical noise heating such as microwave radiation, intrinsic residual heat release from materials used or other heat sources. Considering the high-R junctions and correspondingly weak WF cooling, it is not surprising that EP coupling is dominant here.

When analogously examining the low-R sensors, on the other hand, we find $p = 3.9 \pm 0.4$ and $T_S = 13.4\,\text{mK}$ for the 67 kΩ sensor (see inset Fig. 3), and even $p = 2.7 \pm 0.2$ and $T_S = 6.9 \pm 0.1\,\text{mK}$ for a 134 kΩ sensor (not shown) mounted on a conventional dilution refrigerator (base-$T \sim 5\,\text{mK}$) with improved filtering and chip carrier. Note that T_S is the extrapolated $T_{\text{Cu}} = 0$ saturation-T. The lowest T measured here was $7.5 \pm 0.2\,\text{mK}$. These power-laws far below $p = 5$ indicate that EP cooling is no longer dominant but, rather, a more efficient mechanism $p < 5$ takes over at the lowest-T in the low-R sensors.

In summary, we have demonstrated operation of the NRs down to 0.3 mK while the CBTs cool as low as 7.5 mK. Though the high-R sensor is obviously cooled by EP coupling, the low-R sensors, interestingly, appear to be entering a different cooling regime. However, the low-R sensors have slightly higher T_{CBT} given the same environment, consistent with stronger coupling to the environment. The lowest CBT temperatures are limited by the parasitic heat leak, which is drained by the cooling channels available.

To further improve the sensor performance, the cooling-fin volume can be increased or the heat leak can be reduced, potentially using improvements in microwave shielding and filtering, e.g., using on-chip capacitors, metal planes or alternative array designs. Such efforts will strongly enhance thermalization if a more efficient cooling mechanism is indeed present, since otherwise, in the EP regime, reducing $\dot{Q}_0$ by 5 orders of magnitude will only reduce T_{CBT} by a factor of ten.

An alternative avenue based on quantum dot CBTs, e.g., in GaAs, might also be rewarding, taking advantage of a much larger E_C and level spacing Δ. The resulting reduced sensitivity to the environment might allow a single dot to be used, rather than an array, cooling the reservoirs directly via the WF term, rather than through a long series of junctions.

We would like to thank R. Blaauwgeers, G. Frossati, R. Haley, G. Pickett, V. Shvarts, P. Skyba, and A. de Waard for very useful discussions. This work was supported by the Swiss Nanoscience Institute (SNI), NCCR QSIT, Swiss NSF, ERC starting grant, and EU-FP7 SOLID and MICROKELVIN.

[1] P. Simon and D. Loss, Phys. Rev. Lett. **98**, 156401 (2007).
[2] P. Simon, B. Braunecker, and D. Loss, Phys. Rev. B **77**, 045108 (2008).
[3] R. Hanson, L. P. Kouwenhoven, J. R. Petta, S. Tarucha, and L. M. K. Vandersypen, Rev. Mod. Phys. **79**, 1217 (2007).
[4] C. Nayak, S. H. Simon, A. Stern, M. Freedman, and S. Das Sarma, Rev. Mod. Phys. **80**, 1083 (2008).
[5] A. Stern, Nature (London) **464**, 187 (2010).
[6] O. V. Lounasmaa, *Experimental Principles and Methods Below 1K* (Academic, London, 1974).
[7] F. Pobell, *Matter and Methods at Low Temperatures* (Springer, Berlin, 2007).
[8] G. R. Pickett, Rep. Prog. Phys. **51**, 1295 (1988).
[9] N. Samkharadze, A. Kumar, M. J. Manfra, L. N. Pfeiffer, K. W. West, and G. A. Csáthy, Rev. Sci. Instrum. **82**, 053902 (2011).
[10] W. Pan, J.-S. Xia, V. Shvarts, D. E. Adams, H. L. Stormer, D. C. Tsui, L. N. Pfeiffer, K. W. Baldwin, and K. W. West, Phys. Rev. Lett. **83**, 3530 (1999).
[11] J. Huang, J. S. Xia, D. C. Tsui, L. N. Pfeiffer, and K. West, Phys. Rev. Lett. **98**, 226801 (2007).
[12] A. C. Clark, K. K. Schwarzwälder, T. Bandi, D. Maradan, and D. M. Zumbühl, Rev. Sci. Instrum. **81**, 103904 (2010).
[13] L. Spietz, R. J. Schoelkopf, and P. Pari, Appl. Phys. Lett. **89**, 183123 (2006).
[14] J. P. Pekola, K. P. Hirvi, J. P. Kauppinen, and M. A. Paalanen, Phys. Rev. Lett. **73**, 2903 (1994).
[15] M. Meschke, J. Engert, D. Heyer, and J. P. Pekola, Int. J. Thermophys. **32**, 1378 (2011).
[16] A. B. Zorin, Rev. Sci. Instrum. **66**, 4296 (1995).
[17] C. P. Scheller *et al.* (unpublished).
[18] M. Meschke, J. P. Pekola, F. Gay, R. E. Rapp, and H. Godfrin, J. Low Temp. Phys. **134**, 1119 (2004).